Re–Co/NaY and Re–Co/Al_2O_3 bimetallic catalysts: *in situ* EXAFS study and catalytic activity

D. Bazin [a], L. Borkó [b], Zs. Koppány [b], I. Kovács [b], G. Stefler [b], L.I. Sajó [c], Z. Schay [b], and L. Guczi [b,*]

[a] *LURE, Université de Paris XI, Bâtiment 209D, 91405 Orsay, France*

[b] *Department of Surface Chemistry and Catalysis, Institute of Isotope and Surface Chemistry, CRC HAS, P.O. Box 77, H-1525 Budapest, Hungary*

[c] *Chemical Institute, CRC, HAS, P.O. Box 17, H-1525 Budapest, Hungary*

Received 7 May 2002; accepted 28 August 2002

To reveal possible relations between the structure and catalytic activity, *in situ* EXAFS and catalytic studies complemented with XRD, XPS, and TPR measurements have been performed on the promotion of cobalt catalysts by rhenium prepared by the incipient-wetness technique on Al_2O_3 and NaY zeolite.

In situ EXAFS data collected at the Co K-edge and at the Re L_{III}-edge provided direct evidence of the rhenium–cobalt bond formation. The degree of reducibility depends on the support. There are two structural features, that is, on Re–Co/NaY nearly all rhenium atoms are in contact with Co atoms, whereas the cobalt atoms are surrounded by cobalt atoms in the first coordination sphere. In the case of Re–Co/Al_2O_3 samples the rhenium in oxide form may prevent the development of the "cobalt surface phase" (CSP), which is hardly reducible.

The rate, α value and olefin/paraffin ratio showing special features in the CO hydrogenation and CH_4 conversion to higher hydrocarbons are in line with the structural architecture of the catalysts. Despite the difference in the degree of reducibility, the various activity of Re–Co/NaY and Re–Co/Al_2O_3 may be interpreted by the formation of mixed oxide on alumina preventing the deactivation and agglomeration of small metal particles. Furthermore, the rhenium promotes cobalt activity and the selective formation of higher hydrocarbon. In the mechanism the rhenium also prevents fast deactivation of cobalt.

KEY WORDS: *in situ* EXAFS study; NaY- and Al_2O_3-supported Re–Co; CO hydrogenation; CH_4 conversion.

1. Introduction

The Fischer–Tropsch synthesis offers an attractive route for the production of high-molecular-weight hydrocarbons. One of the most efficient catalysts consists of nanometer-scale metallic Co-based particles deposited in a zeolite supercage [1]. In order to improve cobalt catalytic activity, a second metal is generally added. The influence of the addition of small amounts of other elements such as Gd [2], Zr [3], Ru [4], Pt and Pd to supported cobalt catalysts has been investigated, and also the influence of sol/gel [5] and co-impregnation technique [6] preparation procedures. To explain the effect of the second metal, the existence of a bimetallic cluster is often suggested [6].

Rhenium has been used as a basic additive to Pt/Al_2O_3. The major effect of rhenium in the hydrocarbon reforming technology is to decrease the pressure and temperature during the operation conditions. Simultaneously, deactivation of the reforming catalyst is retarded, thereby elongating the operation time and the catalyst lifetime. Starting from this idea we studied the effect of rhenium on the catalytic activity and selectivity of Fe/Cab-O-Sil in CO hydrogenation. Addition of 10 at% rhenium to iron (total metal loading is 1 wt%) increased the catalytic activity by a 1.5 order of magnitude and affected the olefin selectivity, but in a minor way (it dropped from 90 to 85%) [7,8]. The major effect of rhenium observed was to prevent agglomeration of the small iron particles, measured by Mössbauer spectroscopy. The strong interaction of rhenium oxide hampered migration of the small iron particles to form α-iron, thus preventing the formation of the non-active χ-carbide species. Later, a paper was published using molecular transition metal carbonyl clusters in which a similar effect was discovered [9].

Promotion of rhenium on cobalt catalysts prepared by various methods has been investigated in CO hydrogenation [10]. The Co/NaY and Co/SiO_2 samples including 10 at% rhenium prepared by ion exchange and the sol/gel technique, respectively, were tested. Samples pretreated in various ways revealed an approximately fivefold increase in activity and an increase in the chain length in the NaY-supported sample, while the activity and selectivity changed in various ways in the sol/gel-prepared samples. According to the suggested mechanism, rhenium prevented fast deactivation of cobalt.

In the present paper we wish to provide direct evidence of the formation of heterometallic Co–Re bonds using the *in situ* X-ray absorption technique at the Co K-edge and at the Re L_{III}-edge. The X-ray absorption spectroscopy either at high [11,12] or at low

* To whom correspondence should be addressed.
E-mail: guczi@sunserv.kfki.hu

1011-372X/02/1200-0169/0

energy [13] represents a powerful tool for accessing such information. More precisely, this spectroscopy could be combined with other synchrotron radiation-related techniques such as anomalous wide-angle X-ray scattering (AWAXS) [14], which gives clear structural evidence of the presence of heterometallic bonds, even if metal particles are present in nanometer size [15,16]. We wish to address two problems: first, how the rhenium helps reduction of cobalt ionic species, and second, the role of the support in this process. Based upon these results we wish to elucidate a correlation between the structure of the catalysts and the activity/selectivity revealed in the CO hydrogenation and in the non-oxidative CH_4 conversion to higher hydrocarbons.

2. Experimental

2.1. Catalyst preparation

The samples were prepared by incipient-wetness impregnation over NaY and Al_2O_3 using $Co(NO_3)_3{\cdot}6H_2O$ and $ReCl_3$ aqueous solution, adding rhenium first, then cobalt during the preparation procedure. The total metal loading was 10 wt% and the bimetallic samples contained 10 at% Re. Composition of the catalysts is, for Re-Co/Al_2O_3, Re: 240 μmol g^{-1}, Co: 1064 μmol g^{-1}, and for Re–Co/NaY, Re: 258 μmol g^{-1} and Co: 1110 μmol g^{-1} measured by X-ray flourescence.

2.2. X-ray absorption spectroscopy

In situ X-ray absorption experiments were performed at LURE (Orsay, France), using the DCI storage ring operated with an electron energy of 1.85 GeV and a current between 260 and 360 mA. Data for both Co K-edge (at 7709 eV) and for Re L_{III}-edge (10534 eV) were collected from the beam line placed behind a bending magnet equipped with an Si(111) double crystal monochromator and a boron-silicate double mirror for rejection of harmonics. Ionization chambers filled with air to absorb 20% of the X-ray beam in the first ion chamber and 80% of the X-ray beam in the second ion chamber were used for the measurements in transmission mode. At the Co K-edge (at the Re L_{III}-edge), the estimated energy resolution of the monochromator was approximately 3 eV. The energy/angle calibration was performed using either a Pt foil (thickness 7.5 μm) or a cobalt foil (thickness 7.5 μm) as reference.

After sieving, the particles in the 100–200 μm size range were loaded into a sample holder and placed in a special furnace for *in situ* treatment with entrance and exit windows made of bor-nitride that is transparent to the X-ray beam [17]. Normalized EXAFS spectra were isolated from the experimental data using standard procedures [18]. Data analysis on EXAFS and X-ray absorption near edge structure (XANES) was performed with the use of the "EXAFS pour le Mac" package [19]. Fourier transforms (FT) of the k^3-weighted EXAFS functions were obtained using a Kaiser-type window ranging from 3.0 to 12.0 Å^{-1} beyond the Co K-edge or the Re L_{III}-edge, and calculated without a phase correction. The inverse Fourier transforms (filtered EXAFS) were then obtained in the range between 1.57 and 2.77 Å for Co and between 1.48 and 3.30Å for Re. Metallic cobalt foil was employed as reference for the Co–Co bond characterization [20]. The amplitude and phase associated with Re–Co bonds were evaluated by FeFF 7 [21]. A two-shell least-squares fitting procedure (in k space) using the single scattering EXAFS formulation was applied to calculate the co-ordination number (N), distance (R), and Debye–Waller factor ($\Delta\sigma$). Figures 1 and 2 show the quality of fittings obtained on k and R space for the Re–Co/NaY sample at the

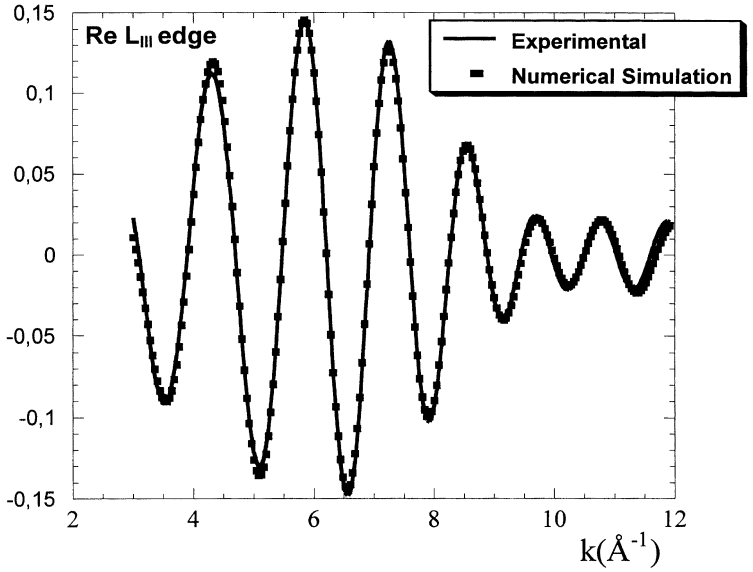

Figure 1. Quality of fitness obtained on the k space for Re–Co/NaY at the Re L_{III}-edge.

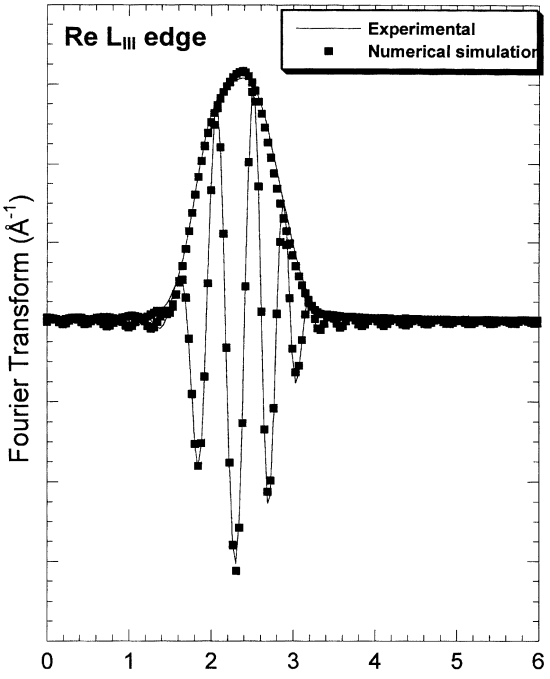

Figure 2. Quality of fitness obtained in the R space for one of the catalysts at the Re L_{III}-edge.

Re L_{III}-edge. Note that this numerical simulation corresponds to a typical residual equal to 10^{-2}. An equivalent value has been obtained for each numerical simulation.

For all simulations the edge shift ΔE was maintained at a value less than 4 eV [22]. The uncertainty in the coordination numbers (ΔN) evaluated from the EXAFS data is usually less than 20% in the most desirable case, for which the least-squares fitting involves only a single coordination shell which is well resolved from its neighboring shells. Following the report of the international workshop on standards and criteria in XAS [23], the error bars on fitted parameters can be estimated by using standard statistical procedures [24]. This procedure indicates an uncertainty for ΔN, which is <1, and more important than the one determined from the data mean standard deviation in $\chi(k)$ using the statexafs code [25]. In fact, we prefer here to validate the EXAFS analysis through high-resolution electron microscopy. This technique was performed on each sample and small metallic clusters were found. This result justifies the EXAFS data analysis procedure. The ultimate goal of the paper is to give structural evidence for the presence or absence of Re–Co bonds and hence obtain a clear chemical description of the system.

2.3. Temperature-programmed reduction, X-ray diffraction, X-ray photoelectron spectroscopy, and catalytic reaction

The samples were characterized by temperature-programmed reduction (TPR) in a flow system using 1 vol% hydrogen/argon mixture with a 10 °C min^{-1} ramp rate with a flow rate of 30 cm^3 min^{-1}.

The X-ray powder diffraction measurements were carried out on a Philips PW1050 goniometer in vertical Bragg–Brentano geometry with a pyrographite monochromator in the scattered beam and a proportional detector using Cu K_α radiation, $\lambda = 1.541862$ Å, an X-ray tube powered by a 3 kW PW1830 generator. The measured files with the collected rough data were evaluated by XDB phase analytical software [26].

X-ray photoelectron spectroscopy (XPS) was a tool to characterize the "as received," calcined and reduced samples using an *in situ* catalytic reactor attached to an XSAM-800 cpi photoelectron spectrometer manufactured by KRATOS. An Al K_α characteristic X-ray line was applied using 80 eV pass energy to measure the cobalt and rhenium spectra. Using a better instrumental resolution resulted in a drastic loss in intensity without significant improvement in spectrum quality. In calculations the Si 2p and Al 2p at 103.3 and 74.4 eV, respectively, were used for reference in the binding energy scale. Sensitivity factors given by the manufacturer were used in the calculations of surface composition. Peak shapes of Co^0 and Co^{2+} were obtained by measuring reference samples of metallic cobalt and Co_2O_3 under the same conditions as the catalysts were measured. These peak shapes and positions were used in the fitting of the Co 2p peak in the catalysts using the XPSPEAK Version 4.1 program.

The CO hydrogenation was carried out in a plug flow reactor working in differential regime in the temperature range 164–253 °C. The Al_2O_3- and NaY-supported bimetallic samples were treated in oxygen at 300 °C for 1 h and in He, respectively, followed by reduction at 400 °C for 2 h. The methane conversion was investigated in a flow system [27]. Generally, 100 mg catalyst was placed into the reactor and one 0.5 cm^3 (22.3 μl) methane pulse was introduced into the system into a stream of helium with a total flow rate of 100 cm^3 min^{-1} at various temperatures. The reaction products were collected in a trap at liquid nitrogen temperature and after warming up they were analyzed. After having the samples analyzed, the catalyst was heated in a stream of hydrogen/helium mixture to 400 °C and then at this temperature the sample was hydrogenated for 1 h and the products were again collected in a cold trap and were analyzed as previously. The unconverted methane was not trapped at liquid nitrogen temperature because no zeolite filling was used.

The products of both reactions were analyzed by means of a CHROMPACK CP 9002 gas chromatograph using a 50 m long plot fused silica column (0.53 mm i.d.) with a stationary phase of CP–Al_2O_3/KCl with a temperature-programmed mode. The rate of CO hydrogenation was measured using 100 mg catalyst at 15 cm^3 min^{-1} flow rate, and was calculated in μmol s^{-1} g_{cat}^{-1}. The methane conversion was characterized by the amount

of C_{2+} products in μmoles (in methane equivalents) related to the amount of catalyst, or the rate was calculated in $\mu mol\,s^{-1}\,g_{cat}^{-1}$ by calculating the contact time from the flow rate and the volume of the methane pulse. Selectivity was calculated by $(C_i/C_{2+}) \times 100$ from $i = 1$–8.

3. Results

3.1. XRD measurements

The XRD results on the Re–Co/NaY and Re–Co/Al_2O_3 samples reduced at 400 °C for 2 h are reported in figure 3. The top, middle and the bottom curves represent the Re–Co/NaY, pure NaY and Re–Co/Al_2O_3 samples, respectively, after treatment first with He (Re–Co/NaY) or O_2 (Re–Co/Al_2O_3) followed by reduction in H_2. The XRD curves for the NaY and Re–Co/NaY samples are identical except for the two lines indicated by asterisks, but these cannot be assigned either to cobalt or to rhenium. The peaks at low Miller indices cannot be seen at all, which indicates the absence of larger crystallites of cobalt and rhenium. Even in the case of bimetallic particles the large-size particles should be under the detection limit, which amounts to about 1%. Similar results are observed for the Re–Co/Al_2O_3 sample because the peaks are characteristic of γ-alumina except for the two lines designated by asterisks. We conclude that small metallic particles exist on both samples and the amount of larger particles is less than 1%.

3.2. Temperature-programmed reduction

Temperature-programmed reduction on the Re–Co/NaY and Re–Co/Al_2O_3 samples is shown in figure 4. In the Re–Co samples prepared by the incipient-wetness technique, a significant reducibility is experienced, much higher than in the case of the same catalysts produced by the sol/gel technique (Re–Co/SiO_2 (SG)) or by ion exchange (Re–Co/NaY (IE)) (35 and 5%, respectively) [28]. The hydrogen uptakes for the Re–Co/Al_2O_3 and Re–Co/NaY samples are 822 and 1470 $\mu mol\,g^{-1}$, respectively. Since on the basis of hydrogen uptake one cannot distinguish between the reducibility of cobalt and rhenium, XPS data are required (see later). Obviously, the high-temperature shift of the TPR peak measured on the Re–Co/Al_2O_3 sample is indicative of the effect of rhenium facilitating cobalt reduction. This is shown by a comparison of the TPR curve for Co/Al_2O_3 in figure 4, similar to earlier results carried out on Co/Al_2O_3, in which the peak temperatures are at 395 and 600 °C [29]. We suggest that the peak at 490 °C corresponds to the Re–Co bimetallic phase, while the peak at 360 °C

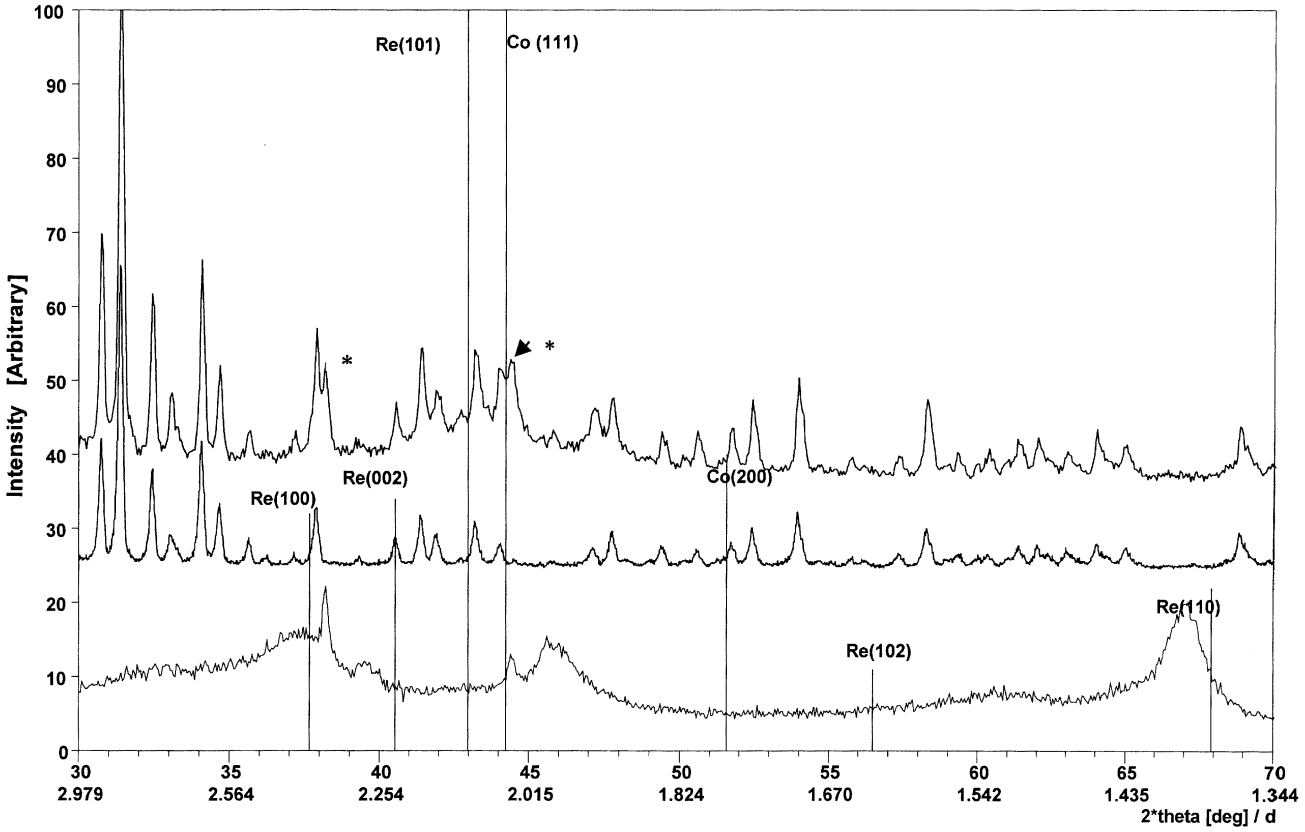

Figure 3. XRD results on Re–Co/NaY sample (top curve), pure NaY zeolite (middle curve) and Re–Co/Al_2O_3 sample (bottom curve) after reduction at 400 °C for 2 h.

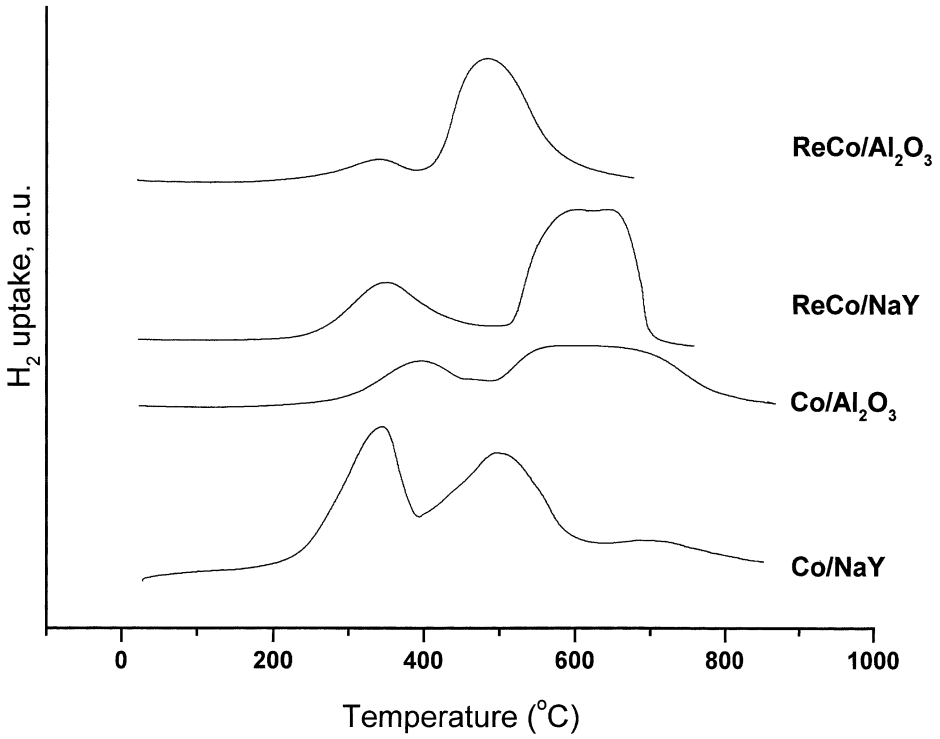

Figure 4. Temperature-programmed reduction of Re–Co/NaY and Re–Co/Al_2O_3 samples after calcination at 300 °C for 1 h.

can be assigned to partial reduction of rhenium which is not interacting with cobalt [7]. However, the data are rather conflicting for the Co/NaY and Re–Co/NaY. The degree of reduction in the latter species is higher than that for Re–Co/Al_2O_3, but it requires somewhat higher temperature. The Co/NaY reduction characteristics depend on the metal loading, because at smaller metal content the TPR temperatures were 520 and 580 °C [30]. It seems plausible to assume that rhenium ionic species is the first impregnating component, spread out at the zeolite surface, thus preventing the formation of large Co-oxide particles that can be reduced easier.

3.3. *In situ EXAFS measurements during reduction*

In the *in situ* cell the sample was first calcined under air at 300 °C for 1 h. After having been flashed by N_2, reduction was carried out under H_2 at 400 °C for 2 h. Then, the data collection was performed at room temperature under H_2 (denoted by A). Sample A was then reoxidized again at 300 °C for 1 h, and the spectra were collected (denoted by B). Finally, the sample re-reduced *in situ* in H_2 at 400 °C for 2 h (denoted by C). All samples were treated in this way for XAF measurement.

3.3.1. *Re–Co/NaY bimetallic samples*

The spectrum was recorded for the Re-Co/NaY sample at the Co K-edge and was taken after reduction.

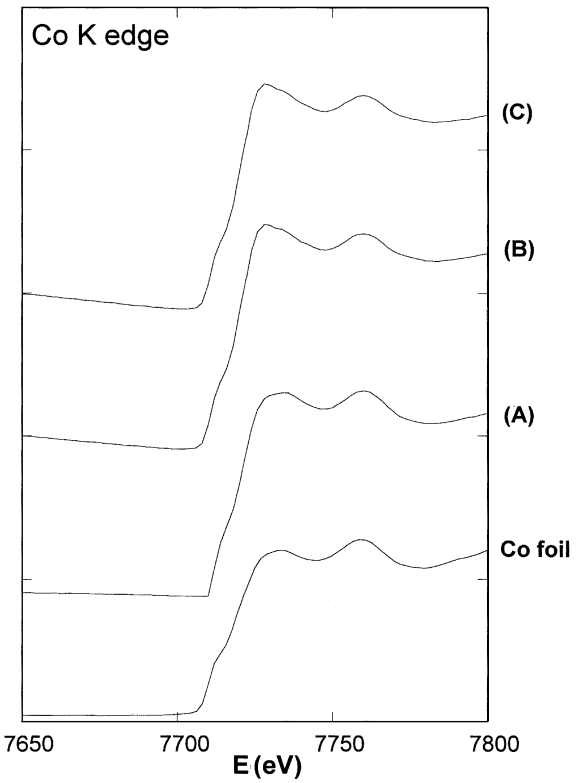

Figure 5. XANES collected at the Co K-edge for the Re–Co/NaY catalyst after the *in situ* reduction (A), after *in situ* air treatment (B) and a second reduction (C) compared to the Co metallic foil (D).

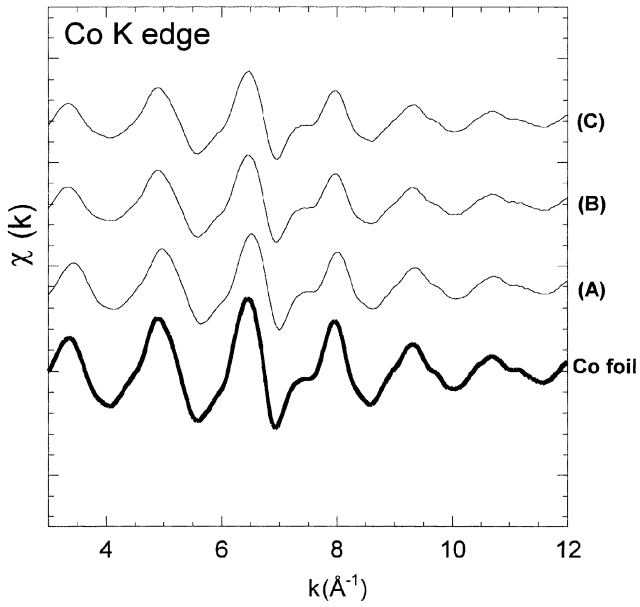

Figure 6. EXAFS data collected at the Co K-edge for the Re–Co/NaY catalyst after the *in situ* reduction (A), after *in situ* air treatment (B) and a second reduction (C) compared to the Co metallic foil (D).

Figure 5 shows the XANES part of the absorption spectrum, which is similar to that of the cobalt foil. A comparison among the EXAFS part of the absorption spectrum (figure 6(A)), the FT module associated with the Co K-edge of the sample (figure 7(A)) and that of metallic cobalt foil (figures 6 and 7) clearly indicates

Table 1
EXAFS analysis performed at the Co K-edge of the Re–Co/NaY sample.

Sample	$N_{Co\text{-}Co}$	$R_{Co\text{-}Co}$	$\Delta\sigma_{Co\text{-}Co}$	$\Delta E_{Co\text{-}Co}$
A	9.0	2.49	0.00	2.1
B	8.0	2.50	0.00	2.1
C	7.9	2.50	0.00	0.1

that the local environment of Co atoms essentially consists of Co atoms. Co–Re bonds do not seem to be present inside the sample, as confirmed by the numerical simulations (table 1).

A similar approach was carried out at the Re L_{III}-edge. The nearest neighbors of the rhenium determined after a numerical simulation of the EXAFS oscillations (EXAFS as well as the modules of the FT modules are shown in figures 8 and 9) are given in table 2. From these results we may conclude that most of the Re atoms are associated with metallic cobalt.

3.3.2. *Re–Co/Al_2O_3 bimetallic samples*

In figure 10 the FT module on the Co K-edge measured on the Re–Co/Al_2O_3 sample is shown. The result clearly indicates that in the first coordination sphere Co atoms surround the cobalt atoms. The calculation shows that $N_{Co\text{-}Co}$ is equal to 8. $R_{Co\text{-}Co} = 2.49$ Å, $\Delta\sigma = 0.03$, $\Delta E = 1.3$. In figure 11 the quality of fitting on the Re L_{III}-edge as a function of k [Å^{-1}] measured on the Re metal and Re–Co/Al_2O_3 sample (solid and dotted lines, respectively) is presented. In figure 12 a

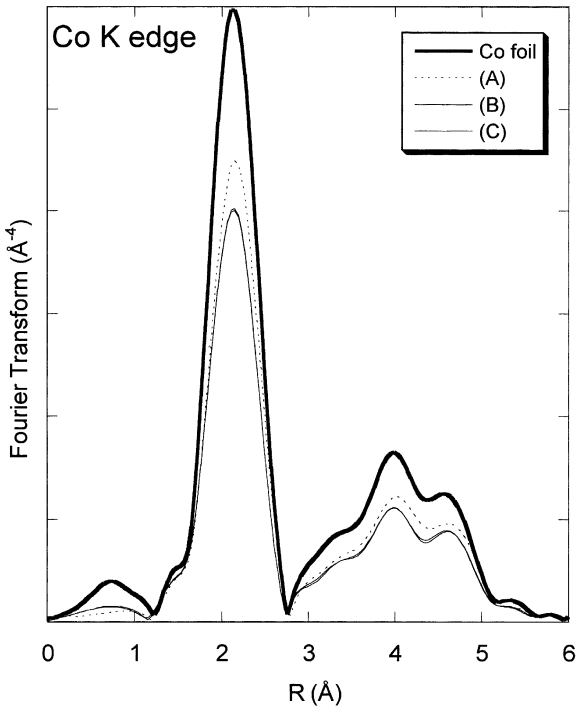

Figure 7. Fourier transform collected at the Co K-edge for the Re–Co/NaY catalyst after the *in situ* reduction (A), after *in situ* air treatment (B) and a second reduction (C) compared to the Co metallic foil (D).

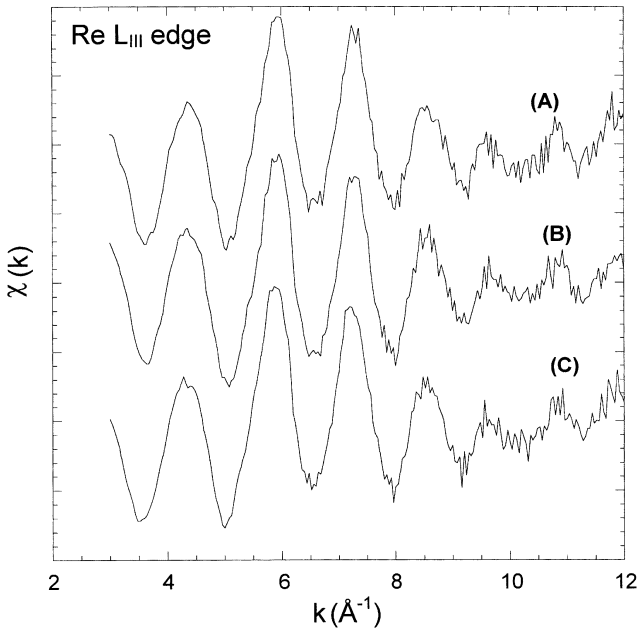

Figure 8. EXAFS collected at the Re L_{III}-edge for the Re–Co/NaY catalyst after the *in situ* reduction (A), after *in situ* air treatment (B) and a second reduction (C).

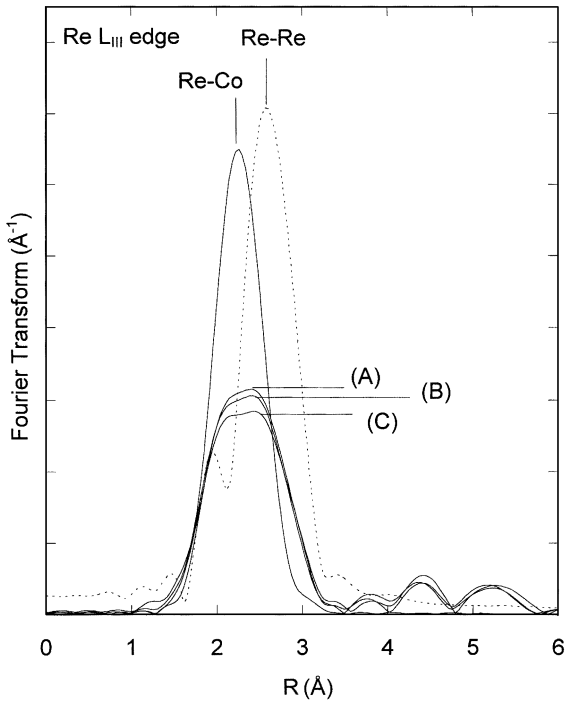

Figure 9. Fourier transform at the Re L_{III}-edge for the Re–Co/NaY catalyst after the *in situ* reduction (A), after *in situ* air treatment (B) and a second reduction (C) compared to the FeFF7 numerical simulations of Re–Co and Re–Re bonds.

comparison is given between the FT performed on Re–Co/Al_2O_3 and Re–Co/NaY samples (dotted and solid lines, respectively). A large difference can be observed between the two samples. While the rhenium in the NaY-supported sample is totally reduced, in the Re–Co/Al_2O_3 sample a part of the rhenium interacts with the alumina support and remains in the oxidized state. The measured coordination numbers and distances are $N_{Re\text{-}Re} = 2.7$, $N_{Re\text{-}Co} = 4$ ($R_{Re\text{-}Co} = 2.5$ Å) and $N_{Re\text{-}O} = 0.6$ ($R_{Re\text{-}O} = 2.02$ Å).

3.4. XPS measurements

XRD already indicated that both in the Al_2O_3 and zeolite samples only nanosize particles are present. In table 3 the XPS data measured under *in situ* conditions on the as-prepared, calcined and reduced samples are presented, and figures 13 and 14 shows the Co 2p and the Re 4f spectra on the reduced samples. From the XPS measurements we know that Re(III) in the as-prepared state is oxidized to Re(VI) with a simultaneous increase of the rhenium surface concentration. However, after reduction Re(VI) is reduced to Re(0) on NaY while on Al_2O_3 0.25 part of Re(VI) is reduced to Re(0) and 0.75 part to Re(IV). The degree of reduction of cobalt

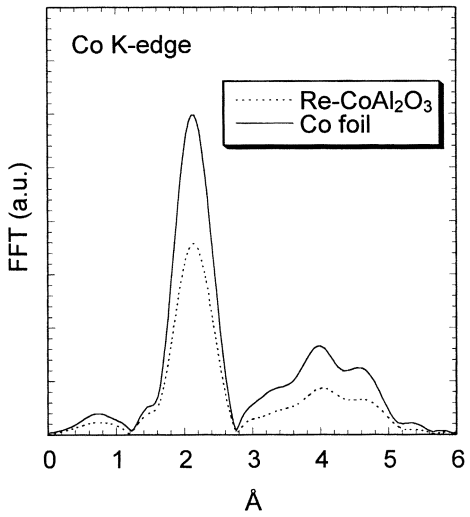

Figure 10. Fourier transform collected at the Co K-edge for the Re-Co/Al_2O_3 catalyst after the *in situ* reduction.

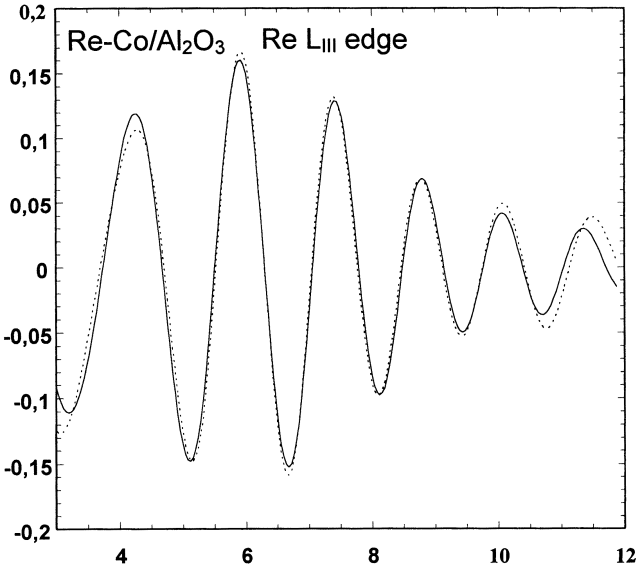

Figure 11. Quality of fitness obtained on the k space for the Re–Co/Al_2O_3 sample at the Re L_{III}-edge.

Table 2
EXAFS analysis performed at the Re L_{III}-edge of the Re–Co/NaY sample.

Sample	$N_{Re\text{-}Re}$	$R_{Re\text{-}Re}$	$\Delta\sigma_{Re\text{-}Re}$	ΔE	$N_{Re\text{-}Co}$	$R_{Re\text{-}Co}$	$\Delta\sigma_{Re\text{-}Co}$	ΔE (eV)
A	3.8	2.690	0.02	5.57	4.0	2.52	0.01	0.2
B	4.2	2.695	0.03	5.90	3.8	2.52	0.00	1.6
C	3.9	2.690	0.03	6.24	3.7	2.51	0.01	1.4

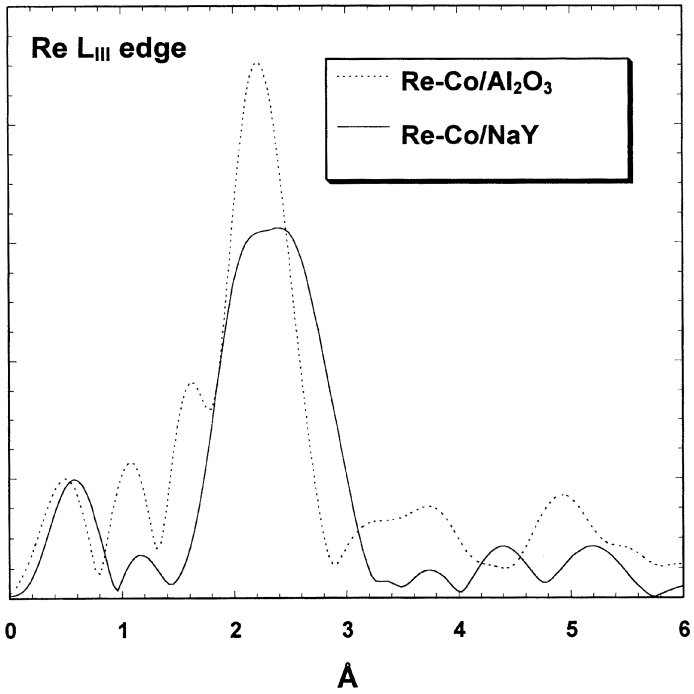

Figure 12. Comparison of the Fourier transform at the Re L_{III}-edge between the Re–Co/NaY (solid lines from figure 9) and the Re–Co/Al_2O_3 catalysts (dotted line) after the *in situ* reduction (A).

calculated by the $Co^0/(Co^0 + Co^{n+})$ ratio is 0.72 ± 0.09 and 0.80 ± 0.1 for the Re–Co/Al_2O_3 and Re–Co/NaY samples, respectively. Furthermore, the rhenium is enriched on the surface of both supports after oxidation to some extent. Its amount decreases after reduction and the Co/Re ratio increases, while on Al_2O_3 both ratios are more or less unchanged.

Considering the hydrogen uptake in the TPR measurements we cannot even roughly estimate the amount of hydrogen used separately for the reduction of cobalt and rhenium (table 4). XPS gives an estimated value for the degree of reduction (column 5 in table 4) and if we used this value the degree of reduction is going to be smaller based upon the TPR data. From both EXAFS and XPS it is unambiguously established that Re is fully reduced on Re–Co/NaY while the reduction is smaller on Re–Co/Al_2O_3. It is, therefore, not irrational to assume that in the Re–Co/NaY sample the overwhelming part of the rhenium is in metallic form and in contact with cobalt as bimetallic particles. On the other hand, in the Re–Co/Al_2O_3 sample a large part of the rhenium and cobalt is in the form of a mixed oxide interacting with alumina. Consequently, the metallic nanoparticles are stabilized by the oxide phase.

3.5. Catalytic reaction

In figure 15 the rates of the CO hydrogenation measured on Re–Co/Al_2O_3 and Re–Co/NaY samples at 10 bar pressures and at various temperatures (top and bottom curves, respectively), along with the selectivity of C_1, C_2–C_4 and C_{5+} species, are plotted. Two prevailing features can be observed. First, with increasing pressure

Table 3
Effect of treatments on surface composition determined by XPS.

Catalyst	Treatment	Co $2p_{3/2}$ (BE/eV)		Re $4f_{7/2}$ (BE/eV)		Re/Co	Co/(Si + Al)	$Co^0/\Sigma Co$	$Re^0/\Sigma Re$
		Co^0	Co_{ox}	Re^0	Re_{ox}				
Re–Co/NaY	As-received	–	782.6	–	46.4	0.057	0.13	–	–
	Air 350 °C	–	780.6	–	45.8	0.049	1.00	–	–
	+ H_2 450 °C	777.7	779.7	40.2	–	0.027	0.70	0.80	1.00
$ReCo/Al_2O_3$	As-received	–	781.5	–	46.2	0.050	0.16	–	–
	Air 350 °C	–	780.9	–	46.1	0.071	0.28	–	–
	+ H_2 450 °C	777.8	779.9	40.6	43.5	0.081	0.12	0.73	0.27

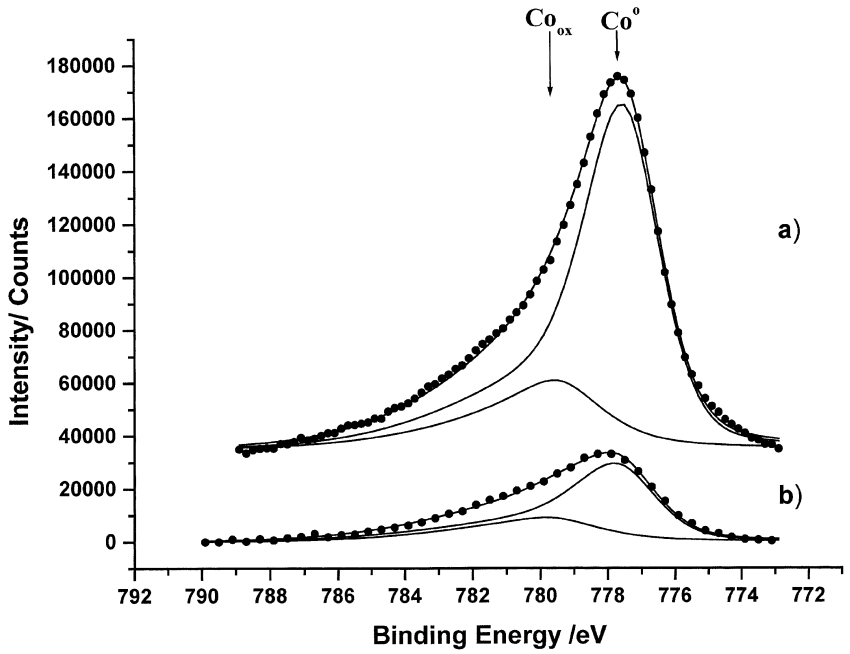

Figure 13. XPS spectra of Co $2p_{3/2}$ for Re–Co/NaY (curve a) and Re–Co/Al_2O_3 (curve b) samples.

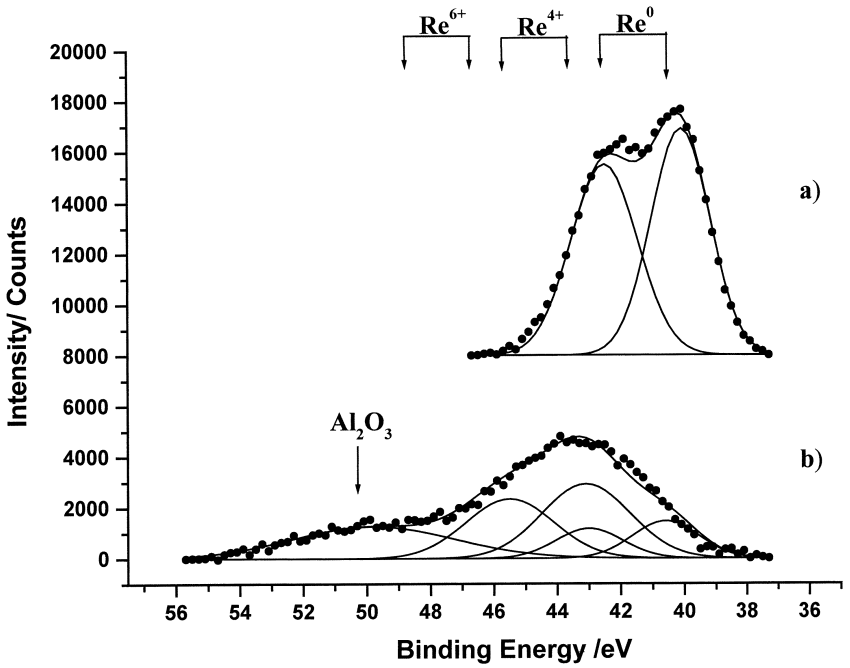

Figure 14. XPS spectra of Re $4f_{7/2}$ for Re–Co/NaY (curve a) and Re–Co/Al_2O_3 (curve b) samples.

Table 4
TPR and XPS data for calculating reducibility of cobalt and rhenium.

Sample	Amount of H_2 uptake (calculated in μmol/g)[a]	Amount of H_2 uptake (by TPR in μmol/g)	Degree of total reduction (TPR)	Degree of Co reduction ($Co^0/\Sigma Co$) by XPS	Degree of Re reduction ($Re^0/\Sigma Re$) by XPS
Co/Al_2O_3	2949	1094	0.38	–	–
Co/NaY	2949	2150	0.74	–	–
$Re–Co/Al_2O_3$	2316	822	0.35	0.72	0.27
Re–Co/NaY	2439	1470	0.60	0.80	1.00

[a] 1 mol Re–3 mol H_2, 1 mol Co–1.5 mol H_2.

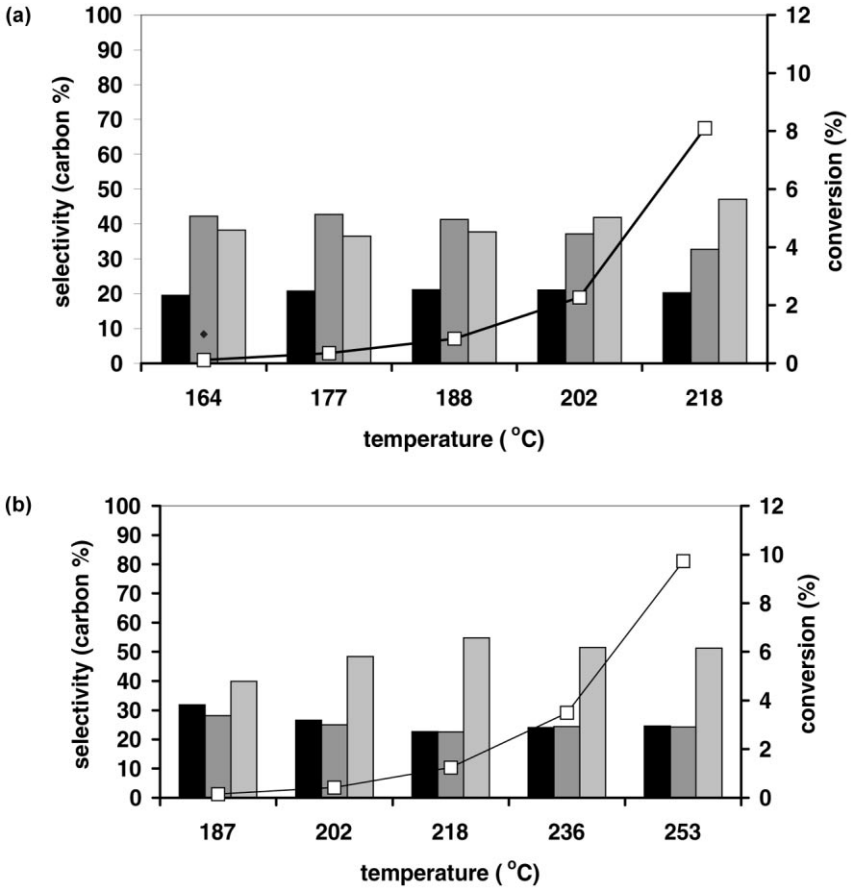

Figure 15. Selectivity and conversion *versus* temperature over Re–Co/Al_2O_3 catalyst (a) and Re–Co/NaY catalyst (b) at 10 bar pressures. Symbols: ■ CH_4, ■ C_2–C_4, ■ C_{5+}.

the C_{5+} selectivity significantly increases (not shown in figure 15) and second, the rates are also enhanced. In the low-temperature range the Re–Co/Al_2O_3 sample is more active than the Re–Co/NaY. This is partly due to retardation of the deactivation processes, as not only is the amount of reduced cobalt in the Re–Co/Al_2O_3 system smaller than in Re–Co/NaY, but the structure is also different. This has been found also in the Re–Fe system [7]. In figure 16 the olefin/paraffin ratios are plotted for both Re–Co/Al_2O_3 and Re–Co/NaY catalysts measured at 218 °C. With increasing pressure the olefin/paraffin ratio drops, indicating the dominance of the hydrogenation steps. However, in the temperature range in which the reaction was performed, the selectivity values do not significantly change. At 1 bar pressure with increasing temperature the methane selectivity

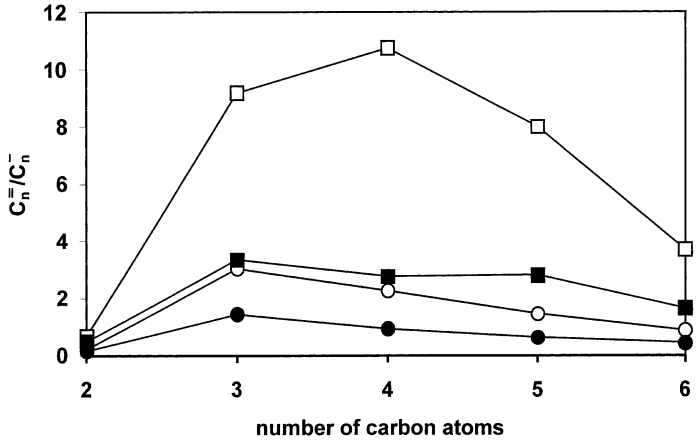

Figure 16. C_n^{2-}/C_n^- ratio measured at 218 °C. Symbols: Re–Co/NaY at 1 bar □ and at 10 bar ■; Re–Co/Al_2O_3 at 1 bar ○ and at 10 bar ●.

Table 5
Rates, energy of activation, α and C_n^{2-}/C_n^- in the CO hydrogenation over various samples at 236 °C at 10 bar pressure.

Samples	Treatment	Rate ($mol\,g_{cat}^{-1}\,s^{-1}$)	E_{act} ($kcal\,mol^{-1}$)	α	C_n^{2-}/C_n^-
Re–Co/Al_2O_3	O_2/300 °C/1 h	7.9×10^{-6}	33.0	0.83	1.10
	+ H_2/400 °C/2 h	1.5×10^{-6} [a]	–	–	n.a.
Re–Co/NaY	O_2/300 °C/1 h	5.7×10^{-7} [a]	32.3	0.97	2.78
	+ H_2/400 °C/2 h	1.4×10^{-6}	–	–	2.19

[a] Measured at 1 bar pressure.

Table 6
Products, selectivity and yield in two-step methane conversion to higher hydrocarbons on supported Re–Co catalysts.

Sample	Products (μmol/g)	$S_{methane}$ (%)	S_{C2+} (%)	C_{2+} yield (%)
Re–Co/Al_2O_3	1.78	26.4	73.6	0.57
Re–Co/NaY	0.52	38.2	61.8	0.14

Pulse mode: step 1: CH_4 activation 250 °C, 100 ml/min, 0.5 ml (23μmol) CH_4 pulse; step 2: CH_x hydrogenation; 250 °C, 100 ml/min H_2, 10 min.

dramatically increases. In table 5 the performances of the various catalysts are compared. As was mentioned, the Re–Co/Al_2O_3 sample is the most active catalyst, but the Re–Co/NaY is better for higher hydrocarbon production. In addition, the latter sample produces the highest olefin/paraffin ratio among the products.

The data for the methane non-oxidative conversion to higher hydrocarbons are presented in table 6. The Re–Co/Al_2O_3 catalyst also seems to be more active, but here the C_{2+} products are higher than on the zeolite-supported catalyst.

4. Discussion

The effect of rhenium has extensively been studied on cobalt-based Fischer–Tropsch (FT) catalysts [31]. Among the new "gas-to-liquid" technologies the "Shell Middle Distillate" technology [32] and the cobalt-based high efficiency Exxon process are worth mentioning [33]. Earlier results have shown that the structure and performance of the Re–Co system strongly depends on the way of preparation. The samples prepared on SiO_2 by the sol/gel technique (Re–Co/SG) or by ion exchange in NaY zeolite Re–Co/NaY (IE) in most cases resulted in the bimetallic nanoparticles [10]. The presence of rhenium measured by XPS is more "visible" in Re–Co/SG than in Re–Co/NaY (IE) catalyst. Although the metal dispersion is high on the Re–Co/SG sample, rhenium is located at the surface in the vicinity of cobalt and XRD shows amorphous Co–Re particles in agreement with TEM measurements which illustrate a highly dispersed metallic cobalt and bimetallic particles (EDX), the average diameter of the metal particles being about 2 nm [34]. On the other hand, the Re–Co/NaY (IM) sample behaves in a different way. XRF indicates that rhenium is present in the sample, but it is not detectable in a measurable quantity at the surface. This is likely because the Re^{3+} ions first exchanged in NaY are mostly covered by the Co^{3+} ions used in the subsequent ion-exchange process. However, its effect is still noticeable as the rate of CO hydrogenation increased by addition of rhenium to cobalt, and the methane, C_2–C_4 and the C_{5+} fractions decreased and increased, respectively. This is why rhenium, similar to other bimetallic systems [7,8,35,36], makes the catalyst more stable against deactivation and increases the catalytic activity.

4.1. Structural modifications induced by rhenium

Generally, from the structural point of view the promoting effects of the Re addition is as follows. (i) Rhenium prevents cobalt agglomeration. Such an effect has been emphasized in the case of Co/Nb_2O_5, similarly to what was observed in the case of iron [7,8]. (ii) Rhenium increases cobalt oxide dispersion during catalyst preparation and promotes the reduction of cobalt oxide to the active metal phase [37]. (iii) It makes the catalyst more stable against deactivation and increases the catalytic activity [7,8,38,39].

In the present work these effects can be clearly visualized. There are characteristic differences between the Re–Co system prepared by the incipient-wetness method and those produced by the sol/gel method or by ion exchange. *In situ* EXAFS experiments provided more information, (i) on the formation of bimetallic clusters, (ii) on the genesis of very small nanometer-scale metallic particles, and (iii) on the decrease of the reduction temperature of the cobalt species.

4.1.1. Re–Co bimetallic nanoparticles

The key issue of the structural study is the *in situ* EXAFS experiments (measured sequentially on the same sample) on the Re–Co/NaY and Re–Co/Al_2O_3 samples at the Co K-edge and the Re L_{III}-edge on the very same sample. At the Re L_{III}-edge, the data analysis unambiguously proved the presence of the Re–Re and Re–Co bonds. However, at the Co K-edge only Co–Co bonds were observed. This is due to the value of the atomic

ratio between the two metals, which is equal to 1/9. Following the simple relationship between coordination number and atomic concentration,

$$C_{Re} \times N_{Re\text{-}Co} = C_{Co} \times N_{Co\text{-}Re},$$

the value calculated for $N_{Re\text{-}Co}$ is too weak to be measured by EXAFS.

In fact, the complete set of data, *i.e.*, the presence of Co–Co, Re–Co and Re–Re interatomic distances, clearly indicates that at least two families of nanoparticles exist inside the catalyst. The first consists of Re–Co bimetallic particles and the second is monometallic Co clusters. Since EXAFS is not a phase-sensitive technique, the presence of Re–Re intermetallic bonds may result from the presence of Re–Co bimetallic nanoparticles or from the presence of Re mono-metallic nanoparticles.

4.1.2. The genesis of very small nanometer-scale metallic particles

We estimated the size of the different nanoparticles of the monometallic Co clusters assuming hcp clusters of spherical morphology. A value of the coordination number between 8 and 9 leads to nanoparticles with a diameter between 1 and 2 nm, respectively. Also, if we consider the signal originating from the upper shell in the FT modules, the particles clearly have an hcp network. If we consider the structural parameters obtained at the Re L_{III}-edge, it seems that the diameter of the bimetallic clusters is close also to the values of 1–2 nm. As pointed out in previous work, it is not possible to calculate the distribution of the two metals inside the bimetallic nanoparticles [15]. Note also that the presence of monometallic Re nanoparticles may affects the size determination.

4.1.3. The decrease of the reduction temperature of the cobalt species

We have evidence that the rhenium promotes cobalt reduction when the metals are in close vicinity to each other, as in Re–Co/Al_2O_3 and Re–Co/SiO_2 prepared by the sol/gel method. Also a high degree of reduction is observed for the Re–Co/NaY sample (80% considering both for Co and Re), whereas the ion-exchanged Re–Co/NaY sample reveals only a small degree of reduction (5%) [10]. That is, if both Re and Co ions are located at the external part of the zeolite and they are in close proximity to each other, the reduction is similar to that observed over both the sol/gel-prepared and the alumina-supported bimetallic samples.

However, a discussion is necessary to explain why Re is not fully reduced on the alumina-supported sample and why the degree of reduction is larger on Re–Co/NaY than on Re–Co/Al_2O_3. In order to understand this phenomenon, we pointed out earlier [8] that an interaction exists between rhenium oxide and other oxide phases, in the present case, alumina. By this interaction the surface sites of alumina are occupied and in strong interaction with rhenium oxide, thus the rhenium reduction is hampered. Consequently, not only migration of the cobalt nanoparticles along the surface is retarded, but the strong cobalt–alumina interaction resulting in the formation of a "cobalt surface phase" (CSP) is also diminished [40]. The latter species forms a monolayer and its reduction requires high temperature. If these bonding sites are already occupied by rhenium oxide the cobalt can more easily be reduced in the presence of rhenium. Nevertheless, the rhenium oxide layer stabilizes small cobalt nanoparticles as was indicated above for the Re–Fe/Cab–O–Sil sample. This is only in line with TiO_2-supported Co–Re catalyst on which the formation and stability of highly dispersed cobalt oxide phase was observed [37]. On the other hand, when rhenium oxide is present only in a small quantity, such as for Re–Co/NaY, not only can rhenium be fully reduced, but also the degree of reduction of cobalt is higher. As was shown also by EXAFS, no signal characteristic of Re–O bonds can be observed.

Hilman *et al.* [41] suggested a somewhat different mechanism using temperature-programmed reduction, namely, reduction of the Co_3O_4 species takes place by hydrogen spillover. The authors also reported that cobalt diffuses into the support during the TPR and not during calcination. Our earlier results were supported by the results of Davis *et al.*, who studied the reduction of Co/Al_2O_3 by TPR [42,43]. These authors found two peaks at 352 and 585 °C, similar to our results. By adding Re to the system in the amount of 0.2, 0.5, and 1.0% the major high-temperature peak shifted to 440, 422, and 376 °C, respectively. We also observed a similar shift, but still a significant amount of cobalt remained in non-alloyed status.

Concerning the structure of the bimetallic catalyst, we have evidence that rhenium promotes cobalt reduction when the metals are in close vicinity to each other, as in Re–Co/Al_2O_3 and Re–Co/SG. Also, a high degree of reduction is observed for the Re–Co/NaY sample, whereas the ion-exchanged Re–Co/NaY sample reveals only a small degree of reduction [10]. That is, if both the Re and Co ions are located at the external part of the zeolite and they are in close proximity to each other, the reduction is similar to that observed over both the sol/gel-prepared and the alumina-supported bimetallic samples.

From this point of view our data do not fully support the work performed by EXAFS by Holmen and coworkers [41], who observed that cobalt ions are reduced first, then rhenium is transferred to the zero oxidation state. From their experiments it follows that pure and cobalt-containing rhenium behave in the same way, but nothing can be concluded for the reducibility of the Co and Co–Re pair. Holmen is most probably right saying that interaction of the cobalt oxide with the support is

so strong that the rhenium oxide is replaced by cobalt oxide and thus rhenium can easily be reduced. Although this explanation might be true (in the case of Fe–Re we indeed found that the strong interaction of rhenium oxide with the SiO_2 support prevents the migration of iron along the surface), the relationship between the reducibility of cobalt alone and rhenium alone was not measured. On the other hand, we have to emphasize that the Re–Re bond distance in table 2 indicates the presence of oxide species, which supports our assumption. However, we agree on the point that bimetallic catalyst is produced and certainly cobalt reduction is promoted by rhenium. The formation of a bimetallic system is further indicated by the high reactivity in the CO hydrogenation (see table 5).

4.2. Rhenium-induced improvement of catalytic properties in CO hydrogenation

The key features of the Re addition to the Co/Al_2O_3 and Co/NaY samples in the CO hydrogenation are the increased activity and C_{5+} selectivity. In the literature the presence of the rhenium in carbon-resistant CO_2–CH_4 reforming catalyst was Re–Pt with 0.5 wt% total metal loading on γ-Al_2O_3 and Pt/(Pt + Re) ratios between 0.2 and 1. Generally Re addition promotes diesel and the gasoline production [44]. The catalysts with low Re content were deactivated very rapidly in the temperature range 600–800 °C due to carbon formation. As the Re content increased, the catalysts became more stable and high conversions were maintained with a Pt/(Pt + Re) ratio of 0.2 for up to 750 h at 800 °C with only minor amounts of carbon formation. Possible explanations for improved stability include the ability of Re to dissociate CO_2, thereby releasing oxygen to remove the carbon. The low-temperature deactivation at high Re content is believed to originate from poisoning of Re atoms by CO_2 molecules that strongly adsorb on the surface [45].

In the CO hydrogenation the olefin/paraffin ratios measured for both Re–Co/Al_2O_3 and Re–Co/NaY samples at 218 °C decrease with increasing pressure [28]. It means that the hydrogenation steps start dominating. However, in the applied temperature range the selectivity values do not significantly change. The Re–Co/Al_2O_3 sample is the most active catalyst, which could be interpreted by the presence of the ReO_x/CoO_x/Al_2O_3 mixed phase. Most likely this phase stabilizes the nanoclusters and prevents the carbon formation, which causes deactivation. Ruckenstein and Wang also suggested such a mechanism for Co/Al_2O_3 catalyst [46].

The feature of the Re–Co/NaY and the ion-exchanged Re–Co/NaY [10] catalyst is quite different. By analogy to the work of Moller and Bein [47], we may assume that Co^{2+} ions are located in the cation exchange position, while the intra-zeolite Re ions are coordinated in the six-member ring. In contrast to the Pd^{2+} ions reported by Moller and Bein, Re ions cannot easily be reduced to promote the Co^{2+} reduction; therefore bimetallic particles are formed in limited amount. This is reflected in the TPR shown earlier, in the XPS spectra in which Re cannot be observed [10], and in the catalytic activity. Since rhenium is not at the same location, its hydrogenation activity is not effective enough, so the olefin/paraffin ratio is high compared with the alumina-supported catalyst, indicating that the metal components are also located in the internal part of the NaY. The Re–Co/NaY is the best for higher hydrocarbon production.

4.3. Methane conversion to higher hydrocarbons

Recently the effect of rhenium was addressed also to low-temperature methane dehydrocondensation to form aromatics [48,49]. It was intriguing to see that deactivation of the catalyst is retarded in the presence of rhenium, similar to that observed in the Re–Fe system. On the other hand, EXAFS experiments were used on Re/HZSM-5 and Mo/HZSM-5 samples to study the active species on methane adsorption at 700 °C. The Re oxide species was converted into metallic rhenium ($R_{Re\text{-}Re} = 2.74$ Å and $N_{Re\text{-}Re} = 4$), whereas Mo oxide was converted into Mo_2C. The authors concluded that the active species was metallic Re in the case of Re/HZSM-5 catalyst.

In the present work, for methane conversion under non-oxidative condition, the alumina-supported sample proved to be far more active than the NaY-supported one. Not only is the yield higher but also the C_{2+} values. Formation of aromatic compounds is negligible due to the non-acidic zeolite.

5. Conclusions

The structure and catalytic activity of the Re–Co bimetallic system prepared by the incipient-wetness technique on Al_2O_3 and NaY zeolite were compared. *In situ* EXAFS studies, XRD and TPR helped us to establish that Re promotes cobalt reduction and that nanometer-scale Re–Co and Co particles are formed.

Formation of the bimetallic particles and the degree of reducibility depend on the support. There are two structural features, that is, on Re–Co/NaY nearly all rhenium atoms are in contact with Co atoms, whereas the cobalt atoms are surrounded by cobalt atoms in the first coordination sphere. In the case of Re–Co/Al_2O_3 samples, a fraction of the rhenium in oxide form prevented the creation of the "cobalt surface phase" (CSP), which is hardly reducible.

The rate, the α value and the olefin/paraffin ratio show that the special features of the CO hydrogenation and CH_4 decomposition are in line with the structural architecture of the catalysts. Rhenium promotes the

cobalt activity and the selective formation of higher hydrocarbon.

Acknowledgments

The authors are indebted to the Hungarian Science and Research Fund (T-34920 and T-030343) for financial support and the COST D15/0005/99 program and the Chemistry Department of the CNRS for supporting the collaborative program with LURE synchrotron facilities.

References

[1] M.E. Dry, in: *Catalysis Sciences and Technology*, eds. J.R. Anderson and M. Boudart, Vol. 1 (Springer Verlag, Berlin, 1981) p. 159.
[2] G.W. Huber, S.J.M. Butala, M.L. Lee and C.H. Bartholomew, Catal. Lett. 74 (2001) 45.
[3] A. Feller, M. Claeys and E. van Steen, J. Catal. 185 (1999) 120.
[4] E. Iglesia, S.L. Soled, R.A. Fiato and G.H. Via, J. Catal. 143 (1993) 345.
[5] K. Okabe, X. Li, T. Matsuzaki, H. Arakawa and K. Fujimoto, J. Sol-Gel Sci. Technol. 19 (2000) 519.
[6] N. Tsubaki, S. Sun and K. Fujimoto, J. Catal. 199 (2001) 236.
[7] Z. Schay, K. Lázár, I. Bogyay and L. Guczi, Appl. Catal. 51 (1989) 33.
[8] Z. Schay, K. Lázár, K. Matusek, I. Bogyay and L. Guczi, Appl. Catal. 51 (1989) 49.
[9] L. Guczi and A. Beck, Polyhedron 7 (1988) 2387.
[10] L. Guczi, G. Stefler, Z. Schay, I. Kiricsi, F. Mizukami, M. Toba and S. Niwa, Stud. Surf. Sci. Catal. 130 (2000) 1097.
[11] D. Bazin, D.A. Sayers and J.J. Rehr, J. Phys. Chem. B. 101 (1997) 11040.
[12] *X-ray Absorption Fine Structure for Catalysts and Surfaces* (ed. Y. Iwasawa) (World Scientific, Singapore, 1996).
[13] L. Guczi and D. Bazin, Appl. Catal. A. 188 (1999) 163.
[14] D. Bazin, L. Guczi and J. Lynch, Appl. Catal. A. in press.
[15] G. Sankar and J.M. Thomas, Topics Catal. 8 (1999) 1.
[16] D. Bazin and L. Guczi, Rec. Res. Dev. Phys. Chem. 3 (1999) 353.
[17] D. Bazin, H. Dexpert and J. Lynch, *In situ XAFS Measurements of Catalysts* in: *X-ray Absorption Fine Structure for Catalysts and Surfaces* (ed. Y. Iwasawa) (World Scientific, Singapore, 1996).
[18] D.E. Sayers and B.A. Bunker, in: *X-ray Absorption: Principles, Applications, Techniques of EXAFS, SEXAFS and XANES* (eds. D.C. Koningsberger and R. Prins), (John Wiley & Sons, New York, 1998) p. 211.
[19] A. Michalowicz, PhD thesis, University of Val de Marne, 1990.
[20] A. Khodakov, J. Lynch, D. Bazin, B. Rebours, N. Zanier, B. Moisson and P. Chaumette, J. Catal. 68 (1997) 16.
[21] J.J. Rehr and R.C. Albers, Phys. Rev. B. 41 (1990) 8149.
[22] A. Michalowicz and G. Vlaic, J. Synch. Rad. News 5 (1998) 1317.
[23] F.W. Lytle, D.E. Sayers and E.A. Stern, Report of the international workshop on standards and criteria in X-ray absorption spectroscopy, Physica, B158 (1989) 701.
[24] P.R. Bevington, *Data Reduction and Error Analysis for the Physical Sciences* (McGraw-Hill, New York, 1992) p. 205.
[25] J.Ph. Piquemal, C. Leroy and A. Michalowicz, unpublished program available on the LURE web-site: www.lure.u-psud;fr, 1999.
[26] I.E. Sajó, Powder Diffraction Phase Analytical System for Windows v2.6, 2000.
[27] L. Guczi, L. Borkó, Zs. Koppány and F. Mizukami, Catal. Lett. 54 (1998) 33.
[28] L. Guczi, G. Stefler, Zs. Koppány and L. Borkó, React. Kinet. Catal. Lett. 74, (2001) 259.
[29] L. Guczi, T. Hoffer, Z. Zsoldos, S. Zyade, G. Maire and F. Garin, J. Phys. Chem. 95 (1991) 802.
[30] G. Lu, T. Hoffer and L. Guczi, Catal. Lett. 14 (1992) 207.
[31] V.M.H. van Wechem and M.M.G. Senden, *Natural Gas Conversion II* (eds. H.E. Curry-Hyde and R.F. Howe), Stud. Surf. Sci. Catal., Vol. 81 (Elsevier, Amsterdam, 1994) p. 43.
[32] B. Eisenberg, R.A. Fiato, C.H. Mauldin, G.R. Say and S.L. Soled, *Natural Gas Conversion V* (eds. A. Parmaliana, D. Sanfilippo, F. Frusteri, A. Vaccari and F. Arena), Stud. Surf. Sci. Catal., Vol. 119 (Elsevier, Amsterdam, 1998) p. 943.
[33] US Patent 4,801,573 (1989).
[34] L. Guczi, G. Stefler, Zs. Koppány, L. Borkó, F. Mizukami, S. Niwa and M. Toba, Appl. Catal. A. submitted for publication.
[35] V.K. Shum, J.B. Butt and W.M.H. Sachtler, J. Catal. 99 (1986) 126.
[36] Z. Schay, K. Matusek and L. Guczi, Appl. Catal. 10 (1984) 173.
[37] C.H. Mauldin and D.E. Varnado, *Natural Gas Conversion VI* (eds. E. Iglesia, J.J. Spivey and T.H. Fleisch) Stud. Surf. Sci. Catal. Vol. 136 (Elsevier, Amsterdam, 2001) p. 417.
[38] V.K. Shum, J.B. Butt and W.M.H. Sachtler, J. Catal. 99 (1986) 126.
[39] Z. Schay, K. Matusek and L. Guczi, Appl. Catal. 10 (1984) 173.
[40] Z. Zsoldos, T. Hoffer and L. Guczi, J. Phys. Chem. 95 (1991) 798.
[41] A.M. Hilman, D. Schanke and A. Holmen, Catal. Lett. 34 (1996) 143.
[42] T.K. Das, Y. Zhang, G. Jacobs, W.A. Conner and B.H. Davis, 17th North American Catalysis Society Meeting, Paper 38, July 3–10, (2001) Toronto, Canada.
[43] G. Jacobs, Y. Zhang, T.K. Das, J. Li and B.H. Davis, 17th North American Catalysis Society Meeting, Poster 83, July 3–10, (2001) Toronto, Canada.
[44] F. Mendes, F.B. Noronha, R.R. Soares, C.A.C. Perez, G. Marcheti and M. Schmal, *Natural Gas Conversion VI* (eds. E. Iglesia, J.J. Spivey and T.H. Fleisch) Stud. Surf. Sci. Catal. Vol. 136 (Elsevier, Amsterdam, 2001) p. 177.
[45] J.T. Richardson, J.-K. Hung and J. Zhao, *Natural Gas Conversion VI.* (eds. E. Iglesia, J.J. Spivey and T.H. Fleisch) Stud. Surf. Sci. Catal. Vol. 136 (Elsevier, Amsterdam, 2001) p. 111.
[46] E. Ruckenstein and H.Y. Wang, J. Catal. 205 (2002) 289.
[47] K. Moller and T. Bein, *Zeolites: Facts, Figures, Future* (eds. P.A. Jacobs and R.A. van Santen), Stud. Surf. Sci. Catal. Vol. 49 (Elsevier, Amsterdam, 1989) p. 985.
[48] Y. Shu and M. Ichikawa, Catal. Today 71 (2001) 55.
[49] R. Onoshi, L. Xu, K. Issoh and M. Ichikawa, *Natural Gas Conversion VI.* (eds. E. Iglesia, J.J. Spivey and T.H. Fleisch), Stud. Surf. Sci. Catal. Vol. 136 (Elsevier, Amsterdam, 2001) p. 393.